Available online at www.sciencedirect.com
ScienceDirect
Trans. Nonferrous Met. Soc. China 25(2015) 3643−3650
Transactions of Nonferrous Metals Society of China
www.tnmsc.cn

Fabrication of $Cu_2O@Cu_2O$ core−shell nanoparticles and conversion to $Cu_2O@Cu$ core−shell nanoparticles in solution

Ai-ling YANG[1], Shun-pin LI[1], Yu-jin WANG[1], Le-le WANG[1], Xi-chang BAO[2], Ren-qiang YANG[2]

1. Department of Physics, Ocean University of China, Qingdao 266100, China;
2. Qingdao Institute of Bioenergy & Bioprocess Technology, Chinese Academy of Sciences, Qingdao 266101, China

Received 19 December 2014; accepted 28 May 2015

Abstract: $Cu_2O@Cu_2O$ core-shell nanoparticles (NPs) were prepared by using solution phase strategy. It was found that $Cu_2O@Cu_2O$ NPs were easily converted to $Cu_2O@Cu$ NPs with the help of polyvinylpyrrolidine (PVP) and excessive ascorbic acid (AA) in air at room temperature, which was an interesting phenomenon. The features of the two kinds of NPs were characterized by XRD, TEM and extinction spectra. $Cu_2O@Cu$ NPs with different shell thicknesses showed wide tunable optical properties for the localized surface plasmon (LSP) in metallic Cu. But $Cu_2O@Cu_2O$ NPs did not indicate this feature. FTIR results reveal that Cu^+ ions on the surface of Cu_2O shell coordinate with N and O atoms in PVP and are further reduced to metallic Cu by excessive AA and then form a nucleation site on the surface of Cu_2O nanocrystalline. PVP binds onto different sites to proceed with the reduction utill all the Cu sources in Cu_2O shell are completely assumed.

Key words: $Cu_2O@Cu_2O$ core−shell nanoparticles; $Cu_2O@Cu$ core−shell nanoparticles; solution phase strategy; reducing agent; tunable optical properties; polyvinylpyrrolidine

1 Introduction

Recently, much attention has been paid to structure controlled nanoparticles (NPs) for morphologies of NPs have important effects on both physical and chemical characteristics, such as mechanical, optical, electrical and magnetic properties [1]. Among various morphologies, core−shell NPs are very significant because of their unique architecture, various properties and enhanced activity [2−8]. Core−shell hybrid NPs represent an important class of multicomponent heterostructured nano systems. Because of the nanoscale interactions between the disparate core and shell components, a combination property from individual components, even enhanced tunability and new synergistic properties will appear [9−12].

Cu and its oxides are low cost and multifunctional materials [13,14], which have attracted great interest due to excellent performance in the fields of electronics [15], photovoltaic [16], catalysis [5], superconductivity [17], magnetic storage [18], electrochemistry [19] and sensing [20]. Cu_2O is a p-type direct band gap semiconductor with a band gap of 2.17 eV. In the past decades, various morphological Cu_2O nanocrystals, such as cubes, octahedron [21], spheres [22], tubes and hollow structures have been synthesized mainly by wet chemical [23,24], electrodeposition [25], solvothermal [22], ultrasound or microwave [26] and laser ablation [27] methods. Cu_2O has large permittivity (ε~7) [5] across the visible and near-infrared regions, when it was used as shell of metal−semiconductor core−shell NPs, there is large red shift of the dipole plasmon resonance. Several research groups [2−5,8,9] fabricated such core-shell NPs and reported related results. $M@Cu_2O$ (M=Au,Ag) core−shell metal−semiconductor NPs [1,3,4,9−12] and M/Cu_2O (M=Ag, Au) heterogeneous nanocrystals are promising to be used as photocatalysis with high efficiencies and sensors with faster response and recovery times. Cu_2O NPs or nanoshells can also be used as templates to synthesize Cu_2S [28] or CuS [29] NPs. For Cu is easily to be oxidized, $Cu@Cu_2O$ (Cu as core and Cu_2O as shell) NPs were easily synthesized [30]. But metal Cu is difficult to obtain by the reduction of copper oxides in solution. In fact, in many cases Cu is expected to play an important role as shell for its high activity in

Foundation item: Projects (41172110, 61107090) supported by the National Natural Science Foundation of China
Corresponding author: Ai-ling YANG; Tel: +86-532-66781208; E-mail: ailingy@ouc.edu.cn
DOI: 10.1016/S1003-6326(15)64005-5

diverse reactions [7] and oxidation free electrode [15] formation in air. So far, few literatures [7,15] reported the successful preparation of Cu_2O@Cu core−shell NPs.

In this work, by using solution strategy, Cu_2O@Cu_2O core−shell NPs could be easily converted to Cu_2O@Cu core−shell NPs with the help of surfactant PVP and reducing agent AA in air at room temperature. By controlling the mole ratio of $Cu(NO_3)_2$ to AA, one can obtain Cu_2O@Cu_2O NPs or Cu_2O@Cu NPs in the same strategy. The features of the two kinds of NPs were characterized by XRD, TEM and extinction spectra. According to the FTIR results, the reason of the conversion was explained.

2 Experimental

2.1 Materials and characterization

Copper chloride dihydrate ($CuCl_2·2H_2O$), copper nitrate hydrate ($Cu(NO_3)·3H_2O$), ascorbic acid (AA, $C_6H_8O_6$), sodium hydroxide (NaOH), ammonium nitrate (NH_4NO_3), PVP (MW=58000) and ethanol were bought from Aladdin. All of the reactants are analytical grade and were used without further purification. The solvent is deionized water.

The crystalline structures of the NPs were identified by a powder X-ray diffractometer (XRD) (Bruker D8 ADVANCE) with Cu K_α radiation (λ=1.5406 Å). The size and morphologies of the NPs were observed by using a transmission electron microscope (TEM, H−7650, Japan). And the UV-Vis absorption spectra and extinction spectra were recorded by an UV-Vis spectrophotometer (Lamda 25, PerkineElmer). FTIR spectroscopy was performed using a Nicolet NI10 FTIR spectrometer.

2.2 Synthesis and characterization

2.2.1 Synthesis of Cu_2O core NPs

The core of Cu_2O NPs was synthesized by using AA as reducer and PVP as stabilizer. Typically, 100 mg PVP was added into 50 mL $CuCl_2$ aqueous solution (1×10^{-4} mol/L) and stirred homogeneously for about 15 min until PVP powder was fully resolved into the solution. Then, 2 mL 0.2 mol/L NaOH solution was added and stirred for 5 min. After that, 2 mL 0.1 mol/L AA was added into the above solution under vigorous stirring for 15 min. The final products were Cu_2O colloid, which will be added into the reactive systems in later fabrication of Cu_2O@Cu_2O and Cu_2O@Cu core−shell NPs.

2.2.2 Synthesis of Cu_2O@Cu_2O and Cu_2O@Cu NPs

Typically, under magnetic stir, 120 mg PVP was resolved into 30 mL aqueous solution containing 0.1305 mol/L $Cu(NO_3)_2·3H_2O$ and 9.625×10^{-4} mol/L NH_4NO_3. Next, 20 mL Cu_2O core colloid was added into above solution. Then, 2.2 mL 0.2 mol/L NaOH was dropwisely added at 1 drop/s of speed and magnetic stirred for 5 min. 2.607 mL 0.1 mol/L AA solution was dropwise added at 1 drop/3s to synthesize Cu_2O@Cu_2O NPs. In this case, the mole ratio of $Cu(NO_3)_2·3H_2O$ to AA is 1:2. When the mole ratio of $Cu(NO_3)_2·3H_2O$ to AA (3.905 mL) is 1:3, Cu_2O@Cu NPs were synthesized. After the complete reaction, the solution was continuously stirred for 5 min. The product was centrifuged and washed with water and ethanol three times to separate the NPs. The final product was dispersed in ethanol and preserved in a refrigerator at 4 °C.

3 Results and discussion

Under alkaline condition, Cu_2O core NPs can be synthesized by AA reducing $CuCl_2$. The reactive process between $CuCl_2·2H_2O$ and AA in the alkaline environment is

$$CuCl_2+2NaOH=Cu(OH)_2\downarrow+2NaCl \quad (1)$$

$$Cu(OH)_2+C_6H_8O_6=Cu_2O\downarrow+C_6H_6O_6+2H_2O \quad (2)$$

When the complete reaction happens, the color of the solution changes from slight blue to slight yellow. Finally, it becomes orange colloid. The crystalline structure of Cu_2O NPs was characterized by XRD. Figure 1(a) shows the XRD pattern of Cu_2O NPs (PDF No. 071−3645). The peaks positioned at 29.50°, 36.34°, 42.29°, 61.31° and 73.48° match well with (110), (111), (200), (220) and (311) planes of the standard data for the face-centered cubic (FCC) structure of Cu_2O. The nanocrystallines grow superiorly along ⟨111⟩ direction. The calculated lattice constant is 4.2741 Å.

Figure 1(b) shows the TEM image of the Cu_2O core NPs. One can see that the shape of the Cu_2O NPs is truncated cubic and the size distribution is in the range of 60−80 nm. The average size of Cu_2O is about 70 nm. At the same time, the Cu_2O NPs have good monodispersity. The reason of the truncated cubic Cu_2O is that PVP molecules are adsorbed onto the {100} facets stronger than that of other facets, leading to the formation of nanocubes with truncated corners mainly bounded by six {100} facets [21].

Figure 1(c) shows the UV-Vis absorption spectrum of the core Cu_2O NPs, indicating that the plasmon absorption peak is at 424 nm.

The synthetic chemistry of Cu_2O shell is also under alkaline condition [10]. After addition of NaOH, nanocrystallines of $Cu(OH)_2$ first form (Eq. (3)). And then these nanocrystallines aggregate on the surfaces of core Cu_2O NPs. For the presence of NH_4NO_3 salt, the rapid growth of the $Cu(OH)_2$ phase is inhibited. And $Cu(OH)_2$ is able to be reversed to $[Cu(H_2O)_6]^{2+}$ (Eq. (4)). And thus, initial clusters and/or crystallites of $Cu(OH)_2$

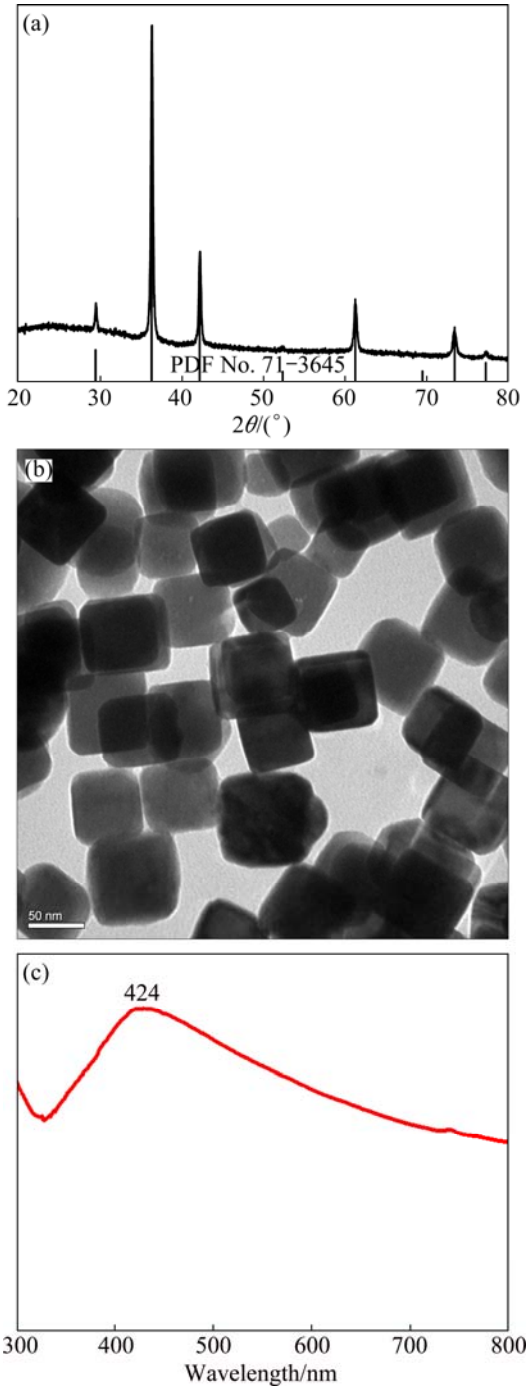

Fig. 1 XRD pattern (a), TEM image (b) and UV-Vis absorption spectrum (c) of Cu_2O core NPs

are solely deposited on the surfaces of core Cu_2O NPs instead of spontaneous crystal growth occurring [10]. Afterwards, with addition of AA, $Cu(OH)_2$ is reduced to Cu_2O (Eq. (5)).

$$[Cu(H_2O)_6]^{2+}+2OH^- \rightleftharpoons Cu(H_2O)_4(OH)_2+2H_2O \quad (3)$$

$$Cu(H_2O)_4(OH)_2+2NH_4^+ \rightleftharpoons [Cu(H_2O)_6]^{2+}+2NH_3\uparrow \quad (4)$$

$$4[Cu(H_2O)_4(OH)_2]+4C_6H_8O_6+O_2 = 2Cu_2O\downarrow+4C_6H_6O_6+24H_2O \quad (5)$$

According to the synthesis steps of Section 2.2.2, when 2.607 mL AA was added into the reactant system (the mole ratio of $Cu(NO_3)_2\cdot 3H_2O$ to AA is 1:2), $Cu_2O@Cu_2O$ core−shell homostructured NPs were fabricated. Figure 2 shows the XRD pattern of $Cu_2O@Cu_2O$ core−shell structure. The five peak positions are as same as Fig. 1(a), which indicates that the nanocrystallines in the shell of Cu_2O also grow superiorly along ⟨111⟩ direction. The core-shell structure was proved by TEM images (Fig. 3)

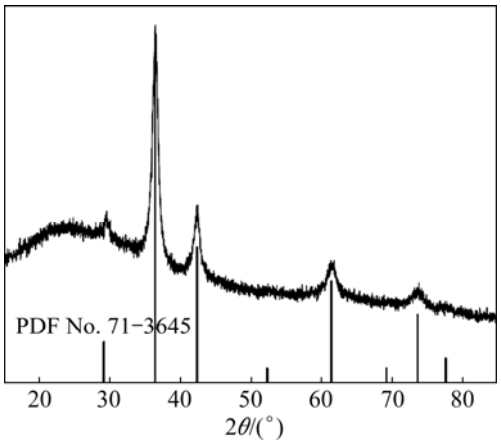

Fig. 2 XRD pattern of $Cu_2O@Cu_2O$ core-shell NPs

For changing the thicknesses of the shells with fixed core size, 35, 30, 20 and 15 mL Cu_2O core colloids were added into the reactant systems containing fixed initial concentrations of Cu^{2+} (0.1184 mol/L) and PVP (0.4%, mass fraction). The addition volumes of AA are the same (2.607 mL). Figure 3 shows the TEM results of $Cu_2O@Cu_2O$ core-shell NPs. The average thicknesses of the shells are respectively 20, 30, 35 and 50 nm in Figs. 3(a)−(d). That is to say, with decreasing addition of Cu_2O core colloids, the thickness of the shells increases and the shells tend to become compact. It is obvious to see that the shells are composed of many small Cu_2O crystallines. For the number of Cu^{2+} is the same as reducer AA in the four reactant systems, the number of reduced Cu^{2+} is also the same, and the more the Cu_2O core NPs, the thinner the shells. It is clear to see the core−shell structure from Fig. 3(a) and Fig. 3(b) for the thinner shells. Comparing Figs. 3(a) and (b) with Fig. 1(b), the cores of the $Cu_2O@Cu_2O$ NPs do not have change after coating. But with the shell thickness increasing, it is difficult to distinguish the core−shell structure (Figs. 3(c) and (d)) for the same composites of core and shell. It is reasonable to infer that the cores of the $Cu_2O@Cu_2O$ NPs in Figs. 3(c) and (d) are also similar to Figs. 3(a) and (b) and do not change after coating.

Figure 4 indicates the normalized extinction spectra of $Cu_2O@Cu_2O$ core−shell NPs when 35, 30, 20 and

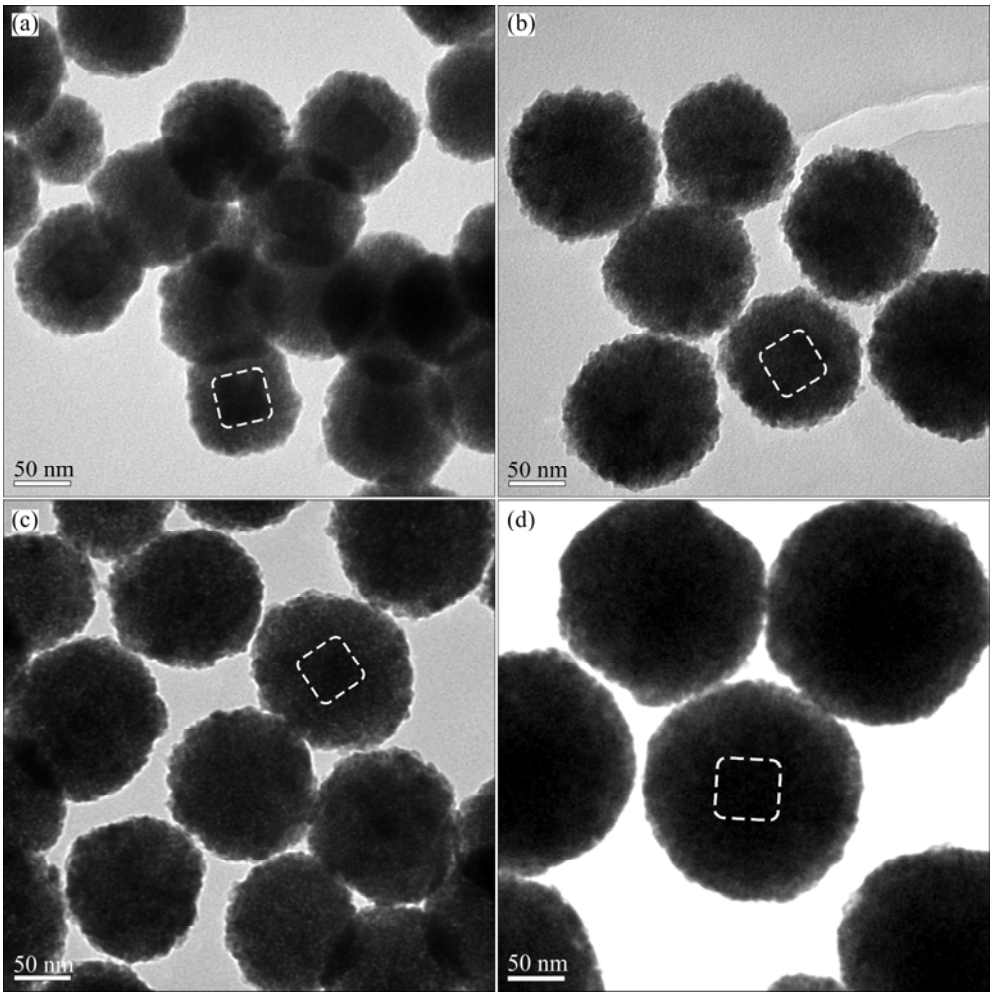

Fig. 3 TEM images of Cu_2O@ Cu_2O core−shell NPs when added 35 mL (a), 30 mL (b), 20 mL (c) and 15 mL (d) Cu_2O core colloids into reactant systems containing fixed initial concentrations of Cu^{2+} and PVP

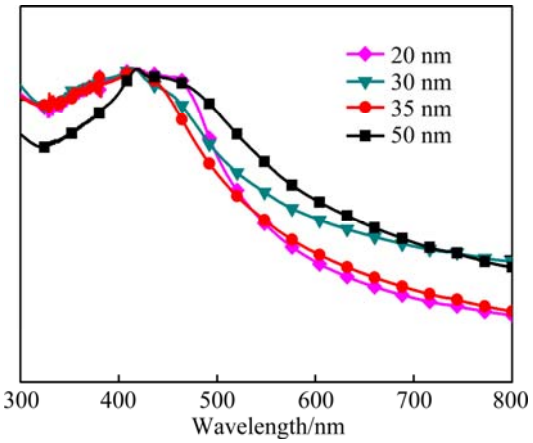

Fig. 4 Extinction spectra of Cu_2O@Cu_2O core-shell NPs with different thicknesses of shells and same size of core (35, 30, 20 and 15 mL Cu_2O core colloids were respectively added into reactant systems with same concentrations of Cu^{2+} and PVP)

15 mL core Cu_2O colloids were added into reactant systems. All the four extinction peaks are near to 424 nm, which is similar to the absorption peak of core Cu_2O NPs (424 nm, Fig. 1(c)). That is to say, the Cu_2O@Cu_2O core-shell NPs do not show optical tenability. The reason is that Cu_2O is semiconductor material, which has weak SPR effect. So, the core−shell structure is equal to increasing the size of the NPs.

In the synthesis process, when the mole ratio of $Cu(NO_3)_2{\cdot}3H_2O$ to AA is 1:3, that is to say, 3.905 mL 0.1 mol/L AA was added into the reactant system, it is found that the final product is Cu_2O@Cu semiconductor−metal NPs, but not Cu_2O@Cu_2O NPs. The XRD experiment proved this result. Figure 5 shows the XRD pattern of the Cu_2O@Cu core-shell semiconductor−metal NPs. There are six peaks at 36.32°, 42.19°, 43.18°, 50.23°, 61.24° and 73.91°, in which, the peaks localized at 36.32°, 42.19° and 61.24° coincide well with (111), (200) and (220) planes of Cu_2O (PDF No. 71−3645), respectively. And the peaks positioned at 43.18°, 50.23° and 73.91° match well with (111), (200) and (220) planes of Cu (PDF No. 70−3038), respectively. So, the product is Cu_2O@Cu core−shell semiconductor−metal NPs, but not Cu_2O@Cu_2O core−shell NPs.

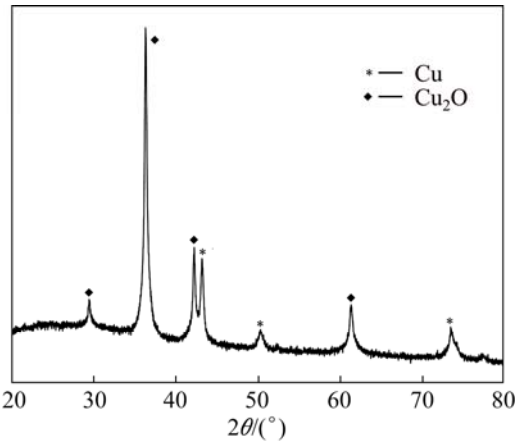

Fig. 5 XRD pattern of core−shell Cu_2O@Cu NPs

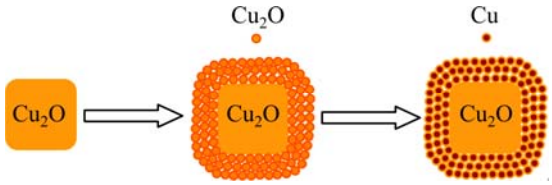

Fig. 6 Schematic diagram of Cu_2O@Cu_2O core−shell NP conversion to Cu_2O@Cu core−shell NP

The reason for the formation of Cu shell could be explained as follows. In the dropwise addition of AA into the coating system (including Cu_2O cores), when the mole ratio of $Cu(NO_3)_2$ to AA reaches 1:2, the Cu^{2+} ions in the reactant system would be firstly reduced to Cu^+ ions, and Cu_2O@Cu_2O NPs would be formed. But at this time, addition of AA was not stopped. That is to say, AA is excessive in the reactant system when the mole ratio of $Cu(NO_3)_2$ to AA is more than 1:2. The Cu^+ ions in the Cu_2O shell would be further reduced by AA and became Cu atoms. When the mole ratio of $Cu(NO_3)_2$ to AA reaches 1:3, all the Cu^+ ions in the shell of Cu_2O would be reduced to Cu atoms, and Cu_2O shell would be converted to Cu shell. Of cause, Cu_2O@Cu_2O NPs would be converted to Cu_2O@Cu NPs. The conversion process is schematically illustrated in Fig. 6. The core−shell structure was proved by TEM. Figure 7 indicates the TEM results as 30 mL (Fig. 7(a)), 20 mL (Fig. 7(b)) and 10 mL (Fig. 7(c)) Cu_2O core colloids were added into the reactant systems containing fixed initial concentrations of Cu^{2+} (0.1305 mol/L) and PVP (0.4%, mass fraction). When 30 mL Cu_2O core colloids were added into the reactant system, the shape of the Cu shell is almost truncated cubes (Fig. 7(a)). And the cores of Cu_2O are nearly not changed in the process of Cu_2O shell converted to Cu shell. The thickness of the shell is about 15 nm. When decreasing addition of the Cu_2O core colloid to 20 mL (Fig. 7(b)), the average thickness of the Cu shells increases to 22 nm. When 10 mL Cu_2O core colloid was added into the reactant system, the average thickness of the shells increases to 30 nm (deduced from the average sizes of core and core−shell NPs), the shape of the shell is approximate to sphere. In this case, the electron beam cannot transmit the NPs, and one cannot distinguish the cores from the NPs (Fig. 7(c)). The Cu shells are composed of many small Cu nanocrystallines with various shapes. The interface between the core of

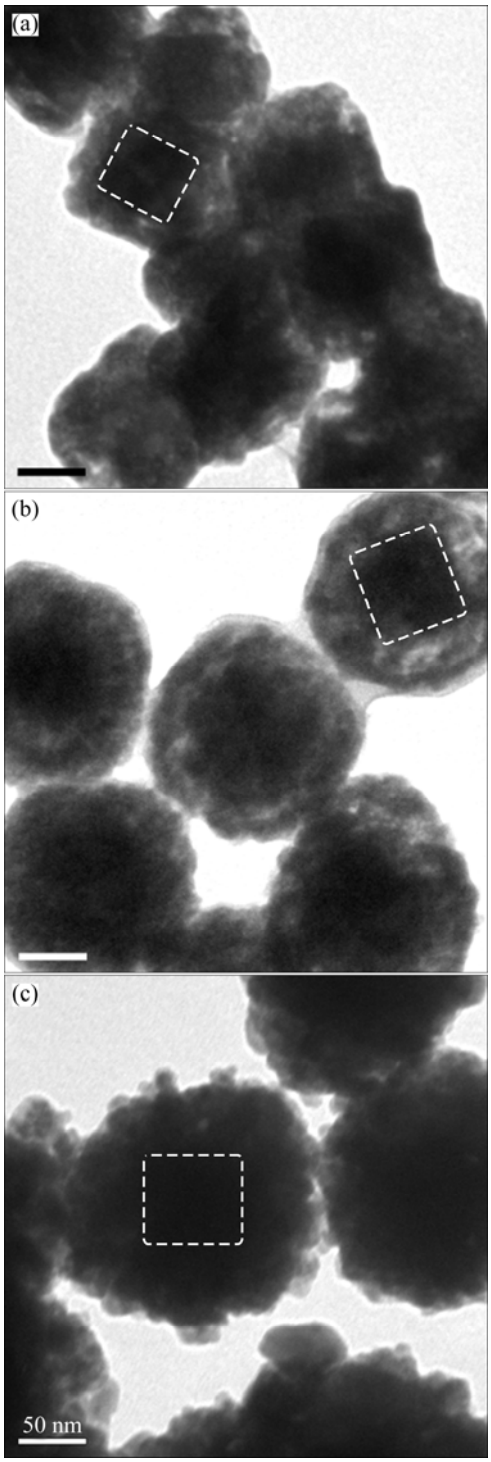

Fig. 7 TEM images of Cu_2O@Cu core−shell NPs with different thicknesses of shells: (a) 15 nm; (b) 22 nm; (c) 30 nm

Cu_2O and the shell of Cu is not compact. Some Cu_2O@Cu NPs are yolk structure. According to Ref. [15], during the conversion, the Cu_2O volume is reduced by 70% to form Cu and make the Cu shell a porous structure.

Figure 8 indicates the extinction spectra of Cu_2O@Cu core-shell NPs with addition of 30, 20, and 10 mL Cu_2O core colloids into the reactant systems. When 30 and 20 mL core Cu_2O colloids were respectively added into the reactive systems, the thicknesses of the Cu shells are thin (15 and 22 nm), and the SPR peaks are at 464 and 480 nm respectively. When the shell thickness increases to 30 nm (10 mL Cu_2O colloid was added into reactant system), except for the peak at 426 nm, there is another extinction peak at 624 nm. The former is attributed to the Cu_2O NPs and Mie scattering of Cu_2O@Cu NPs. The latter is the SPR absorption peak of Cu_2O@Cu. Above results indicate that with the increase of shell thickness, the SPR absorption peaks of the Cu_2O@Cu NPs have red shifts in the range of 40−200 nm. That is to say, by coating Cu_2O NPs with Cu shells, one can obtain NPs with tunable optical properties, which will be promising in optical catalysis or optical devices.

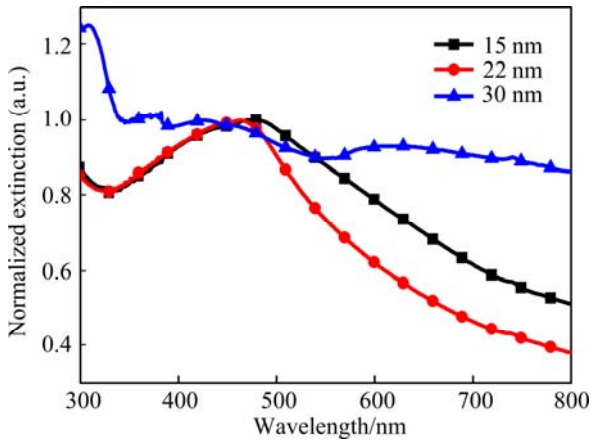

Fig. 8 Extinction spectra of Cu_2O@Cu NPs with different thicknesses of shells and same size of core

According to the above results, one can see that Cu_2O shell could be easily converted to Cu shell in the experimental process when the reducer AA is excessive. LEE et al [15] found crystal-to-crystal conversion of Cu_2O NPs to Cu crystals with polyacrylamide (PAM) as surfactant. Except for PAM, LEE et al [15] tried some other surfactants to prove the role of PAM, but most of them behaved in a different way. So, the shell of Cu_2O converted into Cu shell could not only be related to excessive reductant, but also the surfactant. To probe the interaction between PVP and Cu_2O, FTIR spectra of PVP powder and Cu_2O@Cu_2O NPs were conducted. The FTIR spectra were collected from 32 scans with a resolution of 4 cm^{-1}. The Cu_2O@Cu_2O NPs were desiccated in a vacuum drying oven overnight before measurement. FTIR transmittance spectra of Cu_2O@Cu_2O NPs and PVP powder were measured by preparing thin and transparent KBr pellets containing the materials of interest.

Figure 9 shows the FTIR spectra of pure PVP and Cu_2O@Cu_2O NPs. The broad absorption band at about 3440 cm^{-1} is assigned to the —OH group of H_2O absorbed on the surface of the samples. For the FTIR spectrum of PVP, the absorption band appears at 2953 cm^{-1} corresponding to the stretching vibration of C—H bond. The two bands positioned at 2850 and 2921 cm^{-1} are the symmetric and asymmetric stretching vibration of —CH_2 group, respectively. The strongest absorption band at 1669 cm^{-1} is attributed to the carbonyl group C═O stretching vibration in PVP [30]. The absorption bands positioned at 1289, 1373, 1423, 1463 and 1494 cm^{-1} are assigned to the vibration of heterocyclic [31] in PVP. The bands at 1018, 846, 735, and 650 cm^{-1} are explained by the C—N stretching vibration, out of plane C—H bending, rocking and OH wagging [31], respectively. For the FTIR spectrum of Cu_2O@Cu_2O, the strongest absorption band localized at 626 cm^{-1} is assigned to the Cu — O stretching vibration [32]. Compared the FTIR spectra of Cu_2O@Cu_2O NPs with PVP, it can be seen that the absorption bands positioned at 1018 cm^{-1} and 846 cm^{-1} which are attributed to C—N are red shifted to 1086 cm^{-1} and 856 cm^{-1}. And the band at 1669 cm^{-1} assigned C═O stretching vibration is shifted to low frequency (blue shift) at 1609 cm^{-1}. These shifts indicate the coordination of Cu^+ with N and O atoms in PVP. It was found that gold ion has similar coordination with N and O atoms in PVP [32]. For the N and O atoms in the heterocyclic ring of the PVP structure, the PVP has weak reducing ability [33], and Cu^+ coordinates with N and O atoms in PVP. Under the reduction conditions, the reaction takes place at sites where Cu^+ is adsorbed on the N and O

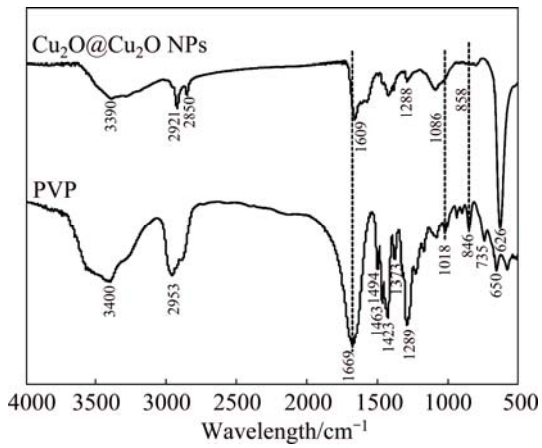

Fig. 9 FTIR spectra of PVP powder and Cu_2O@Cu_2O NPs

atoms (Fig. 10). The main reason for PVP protecting Cu_2O nanocrystallines is N and O in PVP coordinating with Cu^+ and PVP forms the protection layer around the Cu_2O nanocrystallines. In the experimental process, when the reductant of AA is excessive, the Cu^+ ions on the surface of Cu_2O nanocrystallines would be reduced to metallic Cu by AA and then form a nucleation site on the surface of Cu_2O nanocrystalline, PVP binds onto a different site to proceed with the reduction. The crystal growth of Cu is initiated by this nucleation and repeats until all Cu sources in Cu_2O NP are completely assumed. The shell of Cu_2O is converted to Cu shell. And Cu_2O@Cu_2O NPs are converted to Cu_2O@Cu NPs.

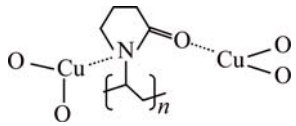

Fig. 10 Schematic diagram of Cu^+ interaction with PVP

4 Conclusions

1) With the help of surfactant PVP and reducing agent AA in air at room temperature, Cu_2O@Cu_2O core-shell NPs were prepared in solution phase strategy. It was found that Cu_2O@Cu_2O NPs were easily converted to Cu_2O@Cu core−shell NPs.

2) The composites, structures, morphologies, extinction properties of Cu_2O@Cu_2O and Cu_2O@Cu core−shell NPs were systematically measured by XRD, TEM and extinction spectra. Cu_2O@Cu_2O core-shell NPs with shell thickness in the range of 20−50 nm do not show tunable optical properties. But the Cu_2O@Cu core−shell NPs show wide tunable optical properties when the shell thicknesses change in the range of 15−30 nm.

3) FTIR results reveal that Cu^+ ions on the surface of Cu_2O shell coordinate with N and O atoms in PVP. The Cu^+ ions are reduced to metallic Cu by excessive ascorbic acid then form a nucleation site on the surface of Cu_2O nanocrystalline. The shell of Cu_2O is converted to Cu shell.

4) The synthesis approach is simple and also a promising reference to synthesize other core-shell NPs with shells of Cu_2O or Cu. The Cu_2O@Cu_2O NPs could be easily converted to Cu_2O@Cu NPs in air at room temperature, which is promising to be used in electronic devices.

References

[1] TSENG C C, HSIEH J H, WU W D. Microstructural analysis and optoelectrical properties of Cu_2O, Cu_2O−Ag, and Cu_2O/Ag_2O multilayered nanocomposite thin films [J]. Thin Solid Films, 2011, 519: 5169−5173.

[2] WANG W C, LYU L M, HUANG M H. Investigation of the effects of polyhedral gold nanocrystal morphology and facets on the formation of Au−Cu_2O core-shell heterostructures [J]. Chemistry Materials, 2011, 23: 2677−2684.

[3] KUO C H, HUA T E, HUANG M H. Au nanocrystal-directed growth of Au−Cu_2O core-shell heterostructures with precise morphological control [J]. American Chemistry Society, 2009, 131: 17871−17878.

[4] LIU De-yu, DING Song-yuan, LIN Hai-xin, LIU Bi-ju, YE Ze-zhong, FAN Feng-Ru, REN Bin, TIAN Zhong-qun. Distinctive enhanced and tunable plasmon resonant absorption from controllable Au@Cu_2O nanoparticles: Experimental and theoretical modeling [J]. Physical Chemistry C, 2012, 116: 4477−4483.

[5] LI J T, CUSHING S K, BRIGHT J, MENG F K, SENTY T R, ZHENG P, BRISTOW A D, WU N Q. Ag@Cu_2O core-shell nanoparticles as visible-light plasmonic photocatalysts [J]. ACS Catalysis, 2013, 3: 47−51.

[6] YEC C C, ZENG H C. Synthetic architecture of multiple core-shell and yolk-shell structures of (Cu_2O@)$n$$Cu_2O$($n$=1−4) with centricity and eccentricity [J]. Chemistry Materials, 2012, 24: 1917−1929.

[7] KOU J H, SAHA A, BENNETT-STAMPER C, VARMA R S. Inside-out core–shell architecture: Controllable fabrication of Cu_2O@Cu with high activity for the Sonogashira coupling reaction [J]. Chemistry Communications, 2012, 48: 5862−5864.

[8] LI Shi-kuo, HUANG Fang-zhi, WANG Yang, SHEN Yu-hua, QIU Ling-guang, XIE An-jian, XU Shou-jiao. Magnetic Fe_3O_4@C@Cu_2O composites with bean-like core/shell nanostructures: Synthesis, properties and application in recyclable photocatalytic degradation of dye pollutants [J]. Materials Chemistry, 2011, 21: 7459−7466.

[9] ZHANG L, BLOM D A, WANG H. Au−Cu_2O core-shell nanoparticles: A hybrid metal-semiconductor heteronanostructure with geometrically tunable optical properties [J]. Chemistry of Materials, 2011, 23: 4587−4598.

[10] ZHANG L, JING H, BOISVERT G, HE J Z, WANG H. Geometry control and optical tunability of metal-cuprous oxide core−shell nanoparticles [J]. ACS Nano, 2012, 6: 3514−3527.

[11] JING H, LARGE N, ZHANG Q F, WANG H. Epitaxial growth of Cu_2O on Ag allows for fine control over particle geometries and optical properties of Ag−Cu_2O core−shell nanoparticles [J]. Physical Chemistry C, 2014, 118: 19948−19963.

[12] LEI Ting. Preparation of novel core-shell nanoparticles by electrochemical synthesis [J]. Transactions of Nonferrous Metals Society of China, 2007, 17(6): 1343−1346.

[13] LIU Na, LI Zhou, LI Ling, LIU Bin, XU Gen-ying. Processing map and hot deformation mechanism of novel nickel-free white copper alloy [J]. Transactions of Nonferrous Metals Society of China, 2014, 24(11): 3492−3499.

[14] VAIRAMANG I, SENTHIL KUMAR T, MALARVIZHI S, BALASUBRAMANIAN V. Application of response surface methodology to maximize tensile strength and minimize interface hardness of friction welded dissimilar joints of austenitic stainless steel and copper alloy [J]. Transactions of Nonferrous Metals Society of China, 2013, 23(8): 2250−2259.

[15] LEE W R, LIM Y S, KIM S, JUNG H, HAN Y K, YOON S, PIAO L H , KIM S H . Crystal-to-crystal conversion of Cu_2O nanoparticles to Cu crystals and applications in printed electronics [J]. Materials Chemistry, 2011, 21: 6928−6933.

[16] MCSHANE C M, CHOI K S. Junction studies on electrochemically fabricated p–n Cu_2O homojunction solar cells for efficiency enhancement [J]. Physical Chemistry & Chemical Physics, 2012, 14: 6112−6118.

[17] PALNICHENKO A V, SIDOROV N S, SHAKHRAI D V, AVDONIN V V, VYASELEV O M, KHASANOV S S. Superconductivity of Cu/CuO_x interface formed by shock-wave pressure [J]. Physica C: Superconductor, 2014, 498: 54−58.

[18] KARAMAT S, RAWAT R S, TAN T L, LEE P, SPRINGHAM S V, REHMAN A, CHEN R, SUN H D. Exciting dilute magnetic semiconductor: Copper-doped ZnO [J]. Superconductor and Novel Magnetism, 2013, 26: 187−195.

[19] HSU Yu-kuei, YU Chun-hao, CHEN Ying-chu, LIN Yan-gu. Hierarchical Cu_2O photocathodes with nano/microspheres for solar hydrogen generation [J]. RSC Advances, 2012, 2: 12455−12459.

[20] CAO Hong-mei, YANG Ai-ling, LI Hua, WANG Le-le, LI Shun-pin, KONG Ji-lie, BAO Xi-chang, YANG Ren-qiang. A non-enzymatic glucose sensing based on hollow cuprous oxide nanospheres in a nafion matrix [J]. Sensors and Actuators B, 2015, 214: 169−173.

[21] SUI Yong-ming, FU Wu-you, YANG Hai-bin, ZENG Yi, ZHANG Yan-yan, ZHAO Qiang, LI Yan-gen, ZHOU Xiao-ming, LENG Yan, LI Ming-hui, ZOU Guang-tian. Low temperature synthesis of Cu_2O crystals: Shape evolution and growth mechanism [J]. Crystal Growth and Design, 2010, 10: 99−108.

[22] PANG Huan, GAO Feng, LU Qing-yi. Glycine-assisted double-solvothermal approach for various cuprous oxide structures with good catalytic activities [J]. Cryst Eng Comm, 2010, 12: 406−412.

[23] YANG Ai-ling, WANG Yu-jin, LI Shun-pin, BAO Xi-chang, YANG Ren-qiang. Stepwise synthesis of cuprous oxide nanoparticles with adjustable structures and growth model [J]. Science China Technological Sciences, 2015, 57(11): 2287−2294.

[24] ZHANG Li, WANG Hui. Cuprous oxide nanoshells with geometrically tunable optical properties [J]. ACS Nano, 2011, 5: 3257−3267.

[25] JIANG Teng-fei, XIE Teng-feng, YANG Wan-shi, CHEN Li-ping, FAN Hai-mei, WANG De-jun. Photoelectrochemical and photovoltaic properties of pn Cu_2O homojunction films and their photocatalytic performance [J]. Physical Chemistry C, 2013, 117: 4619−4624.

[26] HAQUE E, KIM C M, JHUNG S H. Facile synthesis of cuprous oxide using ultrasound, microwave and electric heating: Effect of heating methods on synthesis kinetics, morphology and yield [J]. Crys Eng Comm, 2011, 13: 4060−4068.

[27] LIU Pei-sheng, LI Zhi-gang, CAI Wei-ping, FANG Ming, LUO Xiang-dong. Fabrication of cuprous oxide nanoparticles by laser ablation in PVP aqueous solution [J]. RSC Advances, 2011, 1: 847−851.

[28] KUO Chun-hong, CHU Yi-ting, SONG Yen-fang, HUANG M H. Cu_2O nanocrystal-templated growth of Cu_2S nanocages with encapsulated Au nanoparticles and in-situ transmission X-ray microscopy study [J]. Advanced Functional Materials, 2011, 21: 792−797.

[29] ZHU Hai-tao, WANG Ji-xin, WU Da-xiong. Fast synthesis, formation mechanism, and control of shell thickness of CuS hollow spheres [J]. Inorganic Chemistry, 2009, 48: 7099−7104.

[30] PEDERSEN D B, WANG S L, LIANG S H. Charge-transfer- driven diffusion processes in Cu@Cu-oxide core-shell nanoparticles: Oxidation of (3.0±0.3) nm diameter copper nanoparticles [J]. Physical Chemistry C, 2008, 112: 8819−8826.

[31] SEOUDI R, FOUDA A A, ELMENSHAWY D A. Synthesis, characterization and vibrational spectroscopic studies of different particle size of gold nanoparticle capped with polyvinylpyrrolidone [J]. Physica B, 2010, 405: 906−911.

[32] XU Yan-yan, CHEN Dai-rong, JIAO Xiu-ling, XUE Ke-yan. Nanosized Cu_2O/PEG400 composite hollow spheres with mesoporous shells [J]. Physical Chemistry C, 2007, 111: 16284−16289.

[33] YANG Ai-ling, LI Shun-pin, WANG Yu-jin, WANG Le-le, BAO Xi-chang, YANG Ren-qiang. Synthesis of Ag@Cu_2O core-shell metal-semiconductor nanoparticles and conversion to Ag@Cu core-shell bimetallic nanoparticles [J]. Science China Technological Sciences, 2015, 58: 881−888.

溶液中制备 $Cu_2O@Cu_2O$ 核壳纳米颗粒及其向 $Cu_2O@Cu$ 核壳纳米颗粒的转化

杨爱玲[1]，李顺嫔[1]，王玉金[1]，王乐乐[1]，包西昌[2]，杨仁强[2]

1. 中国海洋大学 物理系，青岛 266100；2. 中国科学院 生物能源与过程研究所，青岛 266101

摘　要：在溶液中制备 $Cu_2O@Cu_2O$ 核壳结构纳米颗粒。在表面活性剂聚乙烯吡咯烷酮(PVP)和过量还原剂抗环血酸(AA)作用下，发现 $Cu_2O@Cu_2O$ 纳米颗粒在室温下易转化为 $Cu_2O@Cu$ 纳米颗粒的有趣现象。采用 XRD、TEM、消光谱表征纳米颗粒的组分、结构、形貌及消光特性。不同壳厚的 $Cu_2O@Cu$ 纳米颗粒由于金属表面等离子体表现出光学调谐特性，但 $Cu_2O@Cu_2O$ 纳米颗粒没有此特性。FTIR 结果表明，Cu_2O 壳表面的 Cu^+与 PVP 中的 N 及 O 结合，进一步被过量的 AA 还原成 Cu 并在 Cu_2O 纳晶表面成核。随着还原的进行，PVP 与 Cu 结合直到 Cu_2O 壳中所有 Cu 源消耗殆尽。

关键词：$Cu_2O@Cu_2O$ 核壳结构纳米颗粒；$Cu_2O@Cu$ 核壳结构纳米颗粒；液相法；还原剂；调谐光学特性；聚乙烯吡咯烷酮

(Edited by Xiang-qun LI)